Mixed Halide Sodalite Solid Solution Systems. Hydrothermal Synthesis and Structural Characterization by Solid State NMR

Henning Trill and Hellmut Eckert*

Institut für Physikalische Chemie, Westfälische Wilhelms Universität Münster, 48149 Münster, Germany

Vojislav I. Srdanov

Department of Chemistry, University of California Santa Barbara, Santa Barbara, California 93106

Received: November 20, 2002; In Final Form: June 3, 2003

The solid solution behavior of mixed halide (Cl/Br, Cl/I, and Br/I) sodalite systems as prepared by hydrothermal synthesis has been studied in detail by X-ray diffraction and solid-state nuclear magnetic resonance (NMR). At a synthesis temperature of 450 K the rate of halide incorporation into the cages of mixed Cl/Br, Br/I, and Cl/I sodalites depends on the halide stoichiometry in the precursor gel and on the particular halogen anion. ^{23}Na and ^{27}Al NMR spectra acquired with magic angle spinning (MAS) are sensitive to both halide composition and distribution and can be used to monitor the onset of phase separation. The Cl/Br and Br/I sodalites show close to ideal miscibility behavior, whereas in the Cl/I sodalites domain segregation effects prevail. The NMR spectra of the quadrupolar ^{23}Na and the halogen nuclei also serve as sensitive indicators of the local symmetry perturbations caused by the disorder inherent to solid solution systems. Furthermore, the continuous variation of lattice parameters in sodalite solid solutions provides an opportunity to probe the fundamental dependence of chemical shift on Na−halogen distances. In this respect the experimental ^{23}Na NMR data reveal an exponential relationship, in agreement with theoretical calculations based on the Hartree−Fock method. In contrast, for the halogen chemical shifts the correlation is found to be approximately linear, with slopes of 17, 35, and 75 ppm/ Å for ^{35}Cl, ^{81}Br, and ^{127}I, respectively. All of these results reflect the high sensitivity of chemical shifts to the extent of anion−cation overlap for nuclei in ionic environments.

I. Introduction

The naturally occurring mineral sodalite is built from an aluminosilicate framework comprised of uniform cages ~6.5 Å in diameter. These are portrayed in Figure 1 as face-sharing truncated octahedra stacked in a space-filling body-centered cubic lattice. In fact, body centering is only preserved in all-siliceous sodalite with $I\bar{4}3n$ symmetry,[1] whereas in an ordered aluminosilicate sodalite of the type described in this study, the lattice symmetry is lowered to $P\bar{4}3n$.[2]

The sodalite cage has T_d point symmetry, with four equivalent sodium cations residing on the body diagonals near the center of the six-membered ring. Even though only three charge-compensating monovalent cations are required per sodalite cage, an excess mineral salt unit, NaX, is typically incorporated. The usual stoichiometry of the sodalite unit cell, taking up the volume of two sodalite cages, is therefore $M_8[Al_6Si_6O_{24}]X_2$ where M is typically an alkali cation and X is a monovalent anion. Sodium chloro sodalite, $Na_8[Al_6Si_6O_{24}]Cl_2$, whose crystal structure was first solved by Pauling,[3] is the only naturally occurring sodalite. Other halogen sodalites can be synthesized via hydrothermal or high-temperature solid-state routes.[4,5] Note that such mixed halide sodalite solid solutions differ from "regular" solid solutions since the mixed species do not directly interact with each other, but their interactions are mediated by the aluminosilicate framework.

In the present work, we will explore how the halide composition obtained in the crystalline material can be controlled by the halide contents in the precursor solution under hydrothermal synthesis conditions. In addition, we will present comprehensive solid-state NMR results on the three mixed halogen sodalite systems (Cl/Br, Br/I, and Cl/I), focusing on

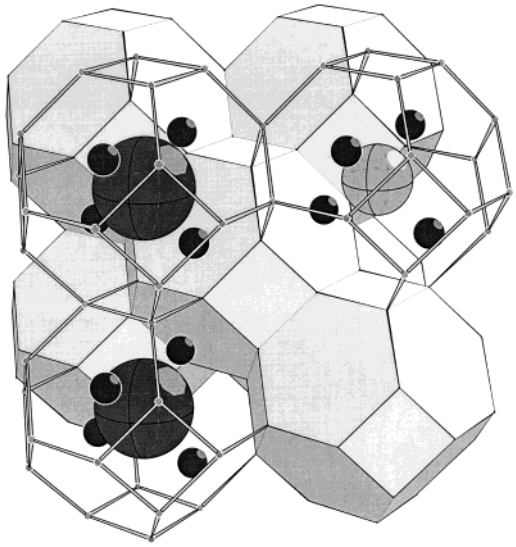

Figure 1. A bcc packing of truncated octahedra representing sodalite cages. The sodalite framework is comprised of regularly alternating AlO_4 and SiO_4 tetrahedra with Al and Si residing at the corners of the truncated octahedra. The extraframework species sodium (small, plain), chlorine (large, bright, crossed), and bromine (large, dark, crossed) are shown in the open cages. Oxygen atoms, each linking two T-sites, are omitted for clarity.

* Corresponding author. E-mail: eckerth@uni-muenster.de.

10.1021/jp0224618 CCC: $25.00
Published on Web 08/05/2003

the influence of the solid solution disorder upon the sodalite framework and the local environment of the extraframework cations. In this connection, the variation of the Na−halogen distance within the three solid solution series provides an opportunity for testing existing theoretical approaches toward a more fundamental understanding of chemical shieldings of nuclei in ionic environments.

II. Experimental Section

The mixed halide sodalites were synthesized in Teflon-coated 20-mL stainless steel autoclaves. The inlays were filled with 3 mmol of calcined kaolin as a precursor, 0.18 mol of NaOH (as Na_2CO_3 free pellets), and 20 mmol of the desired mixture of sodium-halide salts. Distilled water was added to give a total volume of 18 mL and the gel was stirred until all of the sodium hydroxide was dissolved. After stirring for another 30 min the autoclaves were sealed off and heated at 450 K under autogenous pressure for 10 days. After decanting the basic solution, the sodalites were washed several times with distilled water to remove excess sodium hydroxide from the surface of the crystallites.

X-ray diffraction powder patterns in the $12° < 2\theta < 66°$ region were taken with Cu Kα (1.541 78 Å) radiation on a Scintag-X2 diffractometer in 0.02° steps and at a scanning rate of 2 deg/min. Silicon powder was used as an internal standard. The background correction, removal of the Bragg reflections due to the Kα_2 line, and the subsequent determination of the lattice constants by the least-squares procedure was done with the DMSNT 1.37 software package from Scintag. The lattice constants were calculated from the corrected peak data to an accuracy of about 0.001 Å.

^{23}Na, ^{27}Al, ^{35}Cl, ^{81}Br, and ^{129}I magic angle spinning (MAS) NMR spectra were obtained on a Bruker DSX 500 NMR spectrometer at a magnetic field strength of 11.7 T at resonance frequencies of 132.26, 130.28, 49.85, 135.04, and 100.41 MHz, respectively. Complementary experiments were done on Bruker DSX 400 and CXP 200 spectrometers in order to extract chemical shift and quadrupolar coupling parameters from field-dependent spectra. One molar aqueous solutions of $AlCl_3$, NaCl (for both ^{35}Cl and ^{23}Na), NaBr, and NaI were used as 0 ppm chemical shift references. For the halide resonances secondary referencing was done on the basis of solid KCl, KBr, and KI, respectively.

Typical spinning speeds ranged from 10 to 15 kHz. For all samples one-pulse MAS NMR spectra were obtained with 30-deg pulses of 1.0-μs duration. High-resolution triple quantum (TQ) MAS NMR spectra were acquired using the three-pulse sequence with zero quantum filtering.[6,7] For ^{27}Al TQ MAS, the first two hard pulses were 3.8 and 1.4 μs in length, respectively. The third selective 90° pulse had a length of 10 μs. A total of 64−128 spectra, containing 72−144 scans each, were acquired in the F_1 dimension. In the case of ^{23}Na TQ MAS, the first two hard pulses were 3.1 and 1.1 μs in length, respectively. The third selective 90° pulse had a length of 10 μs. A total of 64−128 spectra, containing 48−96 scans each, were acquired in the F_1 dimension.

To obtain insight into the dependence of chemical shielding on Na−halogen distances, the GAUSSIAN-98 program package[8] was used to calculate the ^{23}Na, ^{35}Cl, and ^{81}Br chemical shieldings by the Hartree−Fock method, applying the 6-31G* and the 6-311++G(3df,3pd) basis sets. In the case of iodosodalites, the SDD basis set was applied, which gives similar results as 6-31G* but allows calculation for heavier atoms. The calculation of the NMR parameters proceeded on the basis of molecular fragments based on representative atomic environments. Sodium is coordinated by three oxygen atoms and the halide at the center of the cage. We chose the framework six-ring in which silicon atoms are substituted by aluminum and all open bonds are terminated by hydrogen. This and the halogen anion coordinated by four sodium cations, as shown in Figure 2, was the unit used in most calculations.[9,10] We also evaluated other environments such as Na−halogen "molecules", sodium environments of six rings containing three aluminum ions, and six rings terminated with OH groups. All atomic positions (except for the terminal ions) were computed from the sodalite lattice constant and a fixed Na−O distance, based on the model of Hassan and Grundy.[11] Computations were carried out on environments with and without halide ions and with Na−O distances of either 2.355 or 2.330 Å, corresponding to experimental data for pure halide and pure dry sodalites.[11,12] Only the hydrogen positions were allowed to equilibrate prior to the shielding calculations. For sodium, we found that the variation of basis sets and environments gives results that scatter by ±5 ppm around the values obtained from 6-31G* when the hydrogen-terminated six-ring environment was used. For this reason we choose the latter as a basis for comparison with the experimental results. Shielding calculations of the halide resonances gave only qualitative agreement with experiment even when the 6-311++G(3df,3pd) basis set was applied. On the basis of this result, we speculate that the existing basis sets are optimized for covalent rather than ionic bonds.

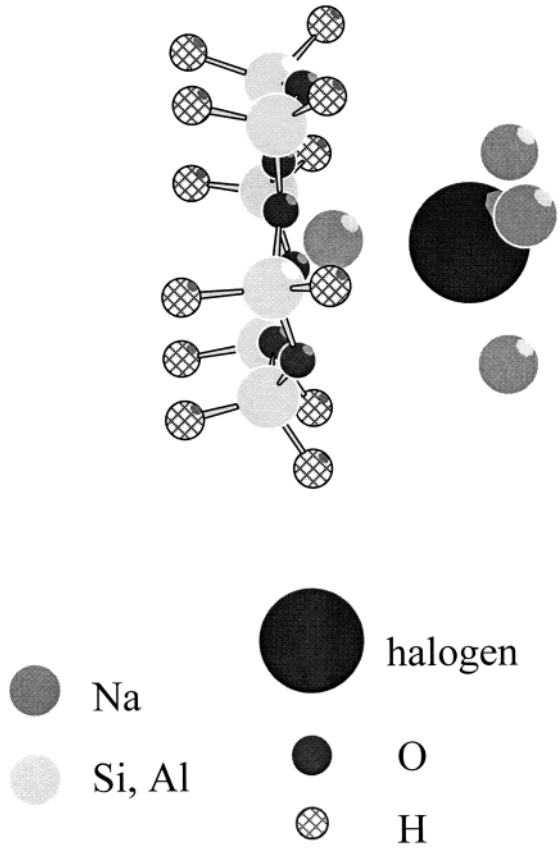

Figure 2. ^{23}Na environment used in most computations. The ^{23}Na nucleus of interest is surrounded by a hydrogen-terminated $(SiO)_6$ ring and by the halide ion with its three additional sodium ligands.

III. Results

Halide Content in Mixed Sodalite. In the hydrothermal synthesis of mixed halide sodalites both halide and $O_2H_3^-$ anions

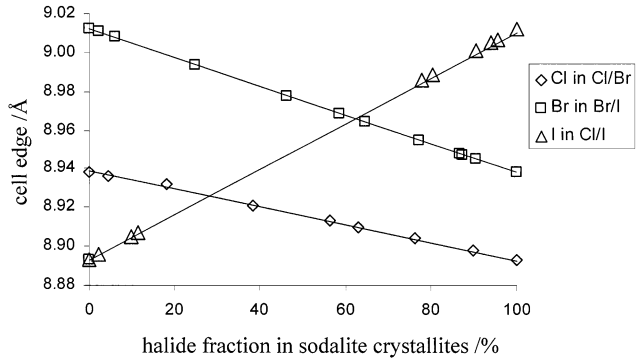

Figure 3. Compositional dependence of the lattice constants in mixed halide sodalites.

compete for the inclusion into the growing sodalite lattice. As shown earlier, the halogen anions are over 100 times more preferred over the $O_2H_3^-$ ions. For the mixed halogen−sodalite solid solution series studied here, we chose a 10-fold excess of the halide source (when compared to the aluminum source) in order to suppress the incorporation of $O_2H_3^-$ ions. A high halide excess in the solution is also necessary to ensure nearly constant halide concentrations during the formation of the sodalite lattice.

For all the mixed Cl/Br and Br/I sodalites, only one set of sharp X-ray diffraction peaks consistent with the $P\bar{4}3n$ space group was found, indicating the absence of phase separation. The experimentally determined unit cell edge for the three solid solution series is plotted as a function of halide content in Figure 3. For the Cl/Br and Br/I series, as well as a part of the Cl/I series, Vegard's rule is obeyed, consistent with the formation of solid solutions. For these samples, the halide contents were determined with an accuracy of 3% using the Vegard relation. The diffraction peaks of mixed Cl/I sodalite samples with comparable Cl and I contents show significant peak broadening, hence indicating the occurrence of domains with different lattice constants. Narrow diffraction peaks suggesting single phase solid solutions are only observed for mixed Cl/I sodalites near the corresponding end-member compositions. Similar observations are made by ^{27}Al NMR (see below).

Plotted in Figure 4 are the halide fractions in mixed sodalites against the respective fractions in the corresponding synthesis solution. While in mixed Cl/Br sodalites, the halide fractions in the sodalite reflect their concentrations in the solution, in Br/I sodalites bromine incorporation appears to be generally favored, except for the sample with the lowest bromine concentration. From Cl and I containing precursor solutions either single phase sodalites with about 90% of the dominant halide are formed or domain separation occurs.

As already demonstrated, the preference for incorporating halide over $H_2O_3^-$ anions into the lattices of mixed halogen/basic sodalites can be described by selectivity factors.[12] $K_{\mathrm{Hal/OH}} = [\mathrm{Hal}]_{\mathrm{solid}}/[\mathrm{Hal}]_{\mathrm{solution}}$. From experimental data obtained on mixed halogen/hydroxide containing gels, we estimate $K_{\mathrm{Cl/OH}} \approx 160$, $K_{\mathrm{Br/OH}} \approx 130$, and $K_{\mathrm{I/OH}} \approx 80$, respectively.[12,13] Based on those one would predict $K_{\mathrm{Cl/Br}} \approx 1.2$, and $K_{\mathrm{Br/I}} \approx 1.6$ in qualitative agreement with the experimental values $K_{\mathrm{Cl/Br}} = 1.0 \pm 0.2$ and $K_{\mathrm{Br/I}} = 1.5 \pm 0.2$ obtainable from the corresponding slopes in Figure 4. For the Cl/I series, this analysis is not appropriate due to the occurrence of phase separation.

NMR Methodology. All of the nuclei examined within the present study have spin quantum number $I > {}^1/_2$ and moderately large nuclear electric quadrupole moments. The effects of nuclear−electric quadrupolar interactions on the MAS NMR line shapes can be calculated by using second-order perturbation

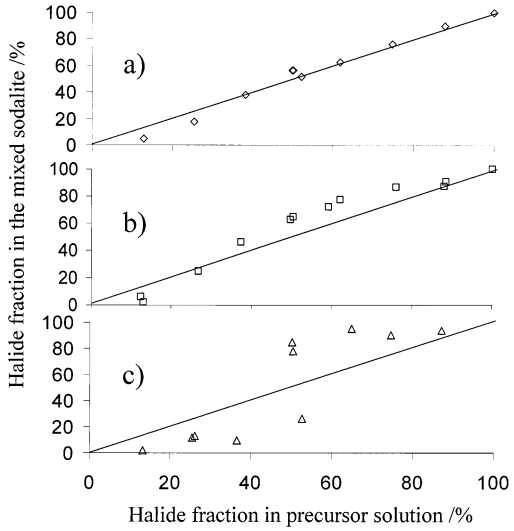

Figure 4. Halide incorporation during the synthesis. The *x*-axes gives the halide fractions in the precursor solutions, while the fractions of the corresponding halide included into the sodalite framework are given on the *y*-axes. (a) Cl^- in Cl/Br sodalites, (b) Br^- in Br/I sodalites, and (c) Cl^- in Cl/I sodalites. Generally more than 98% of sodalite cages are halide-filled. The solid lines represent unity.

theory resulting in anisotropic broadening and shifting of the central $|{}^1/_2> \leftrightarrow |-{}^1/_2>$ coherence. The resonance position is given by

$$\delta_{\mathrm{exp}} = \delta_{\mathrm{cs}} + \delta_{\mathrm{qs}} \tag{1}$$

where δ_{CS} is the chemical shift and the quadrupolar shift (δ_{qs}) is given by[14]

$$\delta_{\mathrm{qs}}(m) = -\frac{3}{40}\frac{I(I+1) - 9m(m-1) - 3}{I^2(2I-1)^2}\frac{{P_{\mathrm{Q}}}^2}{{\nu_0}^2} = -D_I\frac{{P_{\mathrm{Q}}}^2}{{\nu_0}^2} \tag{2}$$

Here ν_0 is the resonance frequency, m is the relevant Zeeman quantum number, and $P_{\mathrm{Q}} = C_{\mathrm{Q}}(1 + \eta^2/3)^{1/2}$ is the quadrupolar coupling parameter with the quadrupolar coupling constant C_{Q} and the asymmetry parameter η. For the central $|1/2> \leftrightarrow |-1/2>$ coherence, the constant D_I only depends on the nuclear spin quantum number I and amounts to 6000 ppm for spin 5/2 nuclei such as ^{27}Al and ^{127}I and 25000 ppm for spin 3/2 nuclei such as ^{23}Na, ^{35}Cl, and ^{81}Br. Since eq 1 implies that the experimental resonance frequency depends on the strength of the applied magnetic field, one can in principle separate the chemical shift and the quadrupolar shift contributions by measuring the spectra at two different Larmor frequencies ${\nu_0}^{\alpha}$ and ${\nu_0}^{\beta}$. From the corresponding resonance shifts δ^{α} and δ^{β} we can determine P_{Q} according to

$${P_Q}^2 = \frac{1}{D_I}\frac{\delta^{\alpha} - \delta^{\beta}}{(1/{\nu_0}^{\beta})^2 - (1/{\nu_0}^{\alpha})^2} \tag{3}$$

Consequently, the isotropic chemical shift is available as well, using eq 1.

Alternatively, triple quantum (TQ) MAS NMR can be used for the same purpose. This method takes advantage of the fact that the angular dependence introduced by first-order quadrupolar coupling is the same for the $|1/2> \leftrightarrow |-1/2>$ and the $|3/2> \leftrightarrow |-3/2>$ coherences. Owing to this fact, the anisotropic second-order quadrupolar broadening can be removed by correlating these two coherences using standard 2D NMR

TABLE 1: Lattice Constants, Calculated Na-Halogen Distances, Halide Contents, and All Chemical Shifts, as Well as Nuclear Electric Quadrupolar Coupling Parameters for the Multinuclear Spectra Displayed in Figures 5−7

mixed Cl/Br sodalites

		^{27}Al				^{23}Na				halides			
Figure 5	Cl, %	a_0, Å	r(Na−Hal), Å	δ, ppm	P_Q, MHz	δ NaCl, ppm	P_Q NaCl, MHz	δ NaBr, ppm	P_Q NaBr, MHz	δ Cl, ppm	P_Q Cl, MHz	δ Br, ppm	P_Q Br, MHz
a	0	8.938	2.857	63.2	0.8			7.2	0.7			−220.6	0.7
b	5	8.936	2.852	63.3	0.7	3.0	0.2	7.2	0.6	−125.4	0.2	−220.8	0.3
c	18	8.932	2.842	63.5	0.8	3.3	0.2	7.5	0.6	−125.2	0.2	−220.5	0.4
b	38	8.921	2.813	63.7	0.8	4.0	0.2	8.4	0.6	−124.7	0.2	−219.4	0.4
e	56	8.913	2.793	63.9	0.8	4.2	0.2	9.1	0.6	−124.3	0.2	−218.6	0.4
f	62	8.910	2.786	64.1	0.9	4.8	0.3	9.3	0.6	−124.1	0.2	−218.3	0.4
g	76	8.904	2.771	64.2	0.9	5.1	0.3	9.8	0.6	−123.8	0.2	−217.7	0.3
h	90	8.898	2.756	64.4	0.9	5.4	0.3	10.2	0.6	−123.6	0.2	−217.3	0.3
i	100	8.893	2.745	64.4	0.7	6.1	0.5			−123.2	0.2		
error	±3	±0.001	±0.004	±0.2	±0.1	±0.2	±0.1	±0.3	±0.1	±0.2	±0.1	±0.4	±0.2

mixed Br/I sodalites

		^{27}Al				^{23}Na				halides			
Figure 6	Br, %	a_0, Å	r(Na−Hal), Å	δ, ppm	P_Q, MHz	δ NaBr, ppm	P_Q NaBr, MHz	δ NaI, ppm	P_Q NaI,MHz	δ Br, ppm	P_Q Br, MHz	δ I, ppm	P_Q I, MHz
a	0	9.012	3.073	61.2	0.6			7.3	1.8			−255.5	1.0
b	6	9.008	3.059	61.3	0.6	3.0	0.6	7.7	1.8	−226. 4	0.7	−255.5	1.1
c	25	8.994	3.015	61.9	0.6	3.9	0.8	9.1	1.7	−225. 0	1.0	−255.2	1.3
d	46	8.978	2.968	62.5	0.7	4.9	0.8	10.8	1.8	−223. 7	0.9	−250.4	2.8
e	65	8.964	2.929	62.8	0.8	5.5	0.7	11.7	1.8	−223. 0	0.8	−250.0	2.6
f	77	8.955	2.903	63.0	0.8	6.1	0.7	12.8	1.8	−222.1	0.8	−247.6	2.1
g	86	8.948	2.884	63.0	0.8	6.7	0.7	13.6	1.8	−222. 0	0.3	−245.5	1.6
h	91	8.947	2.882	63.0	0.8	6.6	0.6	14.1	1.8	−221. 6	0.4	−245.0	1.8
i	100	8.938	2.875	63.2	0.8	7.2	0.6			−220. 6	0.7		
error	±3	±0.001	±0.004	±0.2	±0.1	±0.2	±0.1	±0.3	±0.1	±0.4	±0.2	±0.8	±0.5

mixed Cl/I sodalites

		^{27}Al				^{23}Na					halides		
Figure 7	Cl, %	a_0, Å	r(Na−Hal), Å	δ, ppm	P_Q, MHz	δ NaCl, ppm	P_Q NaCl, MHz	δ NaI, ppm	P_Q NaI,MHz	δ Cl, ppm	P_Q Cl, MHz	δ I, ppm	P_Q I, MHz
a	0	9.012	3.073	61.2	0.6			7.3	1.8			−255. 5	1.0
b	5	9.007	3.056	61.4	0.7	−0.1	0.3	8.2	1.9	−128. 2	0.2	−254.6	1.7
c	6	9.005	3.050	61.4	0.6	−0.4	0.5	8.4	1.7	−128. 7	0.2	−254.4	1.5
d	10	9.001	3.037	61.6	0.7	−0.2	0.4	8.9	1.9	−128. 4	0.2	−253.9	1.8
e	22	8.986	2.991	62.0	0.7	5.2	0.5	10.3	2.0	−124. 1	0.2	−254.8	2.3
g	90	8.905	2.773	64.2	0.9	5.8	0.6	17.0	2.1	−123.8	0.2	−227.1	3.9
f	89	8.907	2.778	64.2	1.0	5.9	0.6	18.0	2.1	−123. 7	0.2	−228.2	4.3
h	97	8.896	2.751	64.4	0.9	5.9	0.5	19.0	2.1	−123. 4	0.2		
i	100	8.893	2.745	64.4	0.7	6.1	0.4			−123. 2	0.2		
error	±3	±0.001	±0.004	±0.2	±0.1	±0.2	±0.1	±0.3	±0.1	±0.3	±0.1	±0.8	±0.5

methodology. After a shearing transformation with appropriate scaling,[15] the projection of the F_2 dimension corresponds to the regular 1D spectra, while the projection in the F_1 dimension is devoid of anisotropic broadening. The isotropic chemical shift, δ_{cs}, can be calculated from the shifts in the F_1 and F_2 dimensions, δ_{F_1} and δ_{F_2},

$$\delta_{cs} = \frac{17\delta_{F_1} + 10\delta_{F_2}}{27} \quad (4)$$

Table 1 summarizes the interaction parameters for all nuclei, determined by the above procedures for the samples under study.

^{27}Al MAS NMR. As can be seen from Figures 5A−7A all of the samples of the Cl/Br and Br/I sodalite series show single ^{27}Al NMR resonances, which vary only slightly in shift and line width. The quadrupolar coupling parameters P_Q, determined from field-dependent measurements, scatter around 0.8 MHz and are in agreement with values for pure halide sodalites.[16] For all the solid solution series, the ^{27}Al chemical shifts vary linearly with the lattice constant. For some mixed Cl/I sodalites we observe two resonances. From the ^{27}Al TQ MAS NMR spectra in Figure 8, which belong to a sodalite sample with a Cl/I ratio close to unity, it was found that the two resonances have chemical shifts and quadrupolar coupling constants close to the values of pure chloro- and iodo-sodalite.[16] This indicates an onset of phase separation characterized by domain segregation, in agreement with the X-ray data shown earlier. Apparently, the different sizes of the halogen anions would inflict a large strain on the aluminosilicate framework if these were incorporated randomly, thus phase separation is preferred.

^{23}Na MAS NMR. The ^{23}Na MAS NMR spectra of the three series of mixed halide sodalites are shown in Figures 5B−7B. In the Cl/Br series two sodium resonances are clearly separated from each other. Based on the compositional evolution of their intensities, it is obvious that the high-frequency resonance has to be assigned to sodium in bromo cages, while the low-frequency resonance originates from sodium in chloro cages. The quadrupolar coupling constants are about 0.8 and 0.4 MHz for the high- and low-frequency resonance, respectively, and scatter by only 0.1 MHz throughout the whole series. Besides the variation in intensity, we observe a variation of the chemical shift with composition. As the lattice constant increases, both ^{23}Na resonances are shifted to lower resonance frequencies.

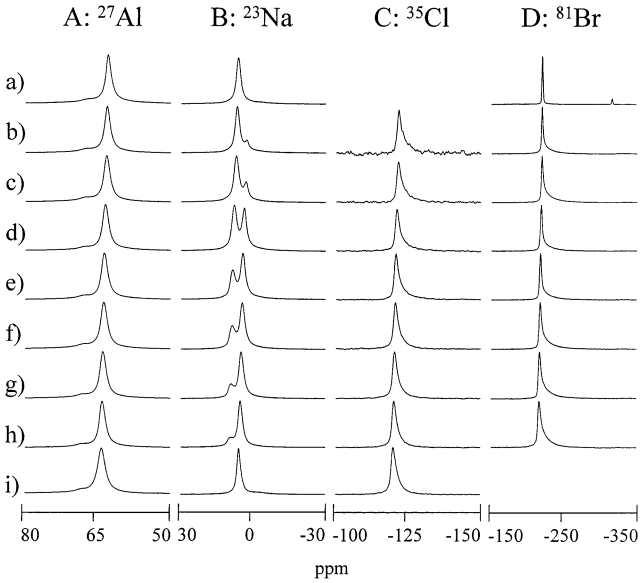

Figure 5. ^{23}Na, ^{27}Al, ^{35}Cl, and ^{81}Br MAS NMR spectra of mixed Cl/Br sodalites. The spectra were taken in a 11.7 T magnetic field at spinning speeds of 10 kHz. The sodalite cages are over 98% occupied by halide ions of which (a) 0%, (b) 5%, (c) 18%, (d) 38, (e) 56%, (f) 62%, (g) 76%, (h) 90%, and (i) 100% are Cl^-.

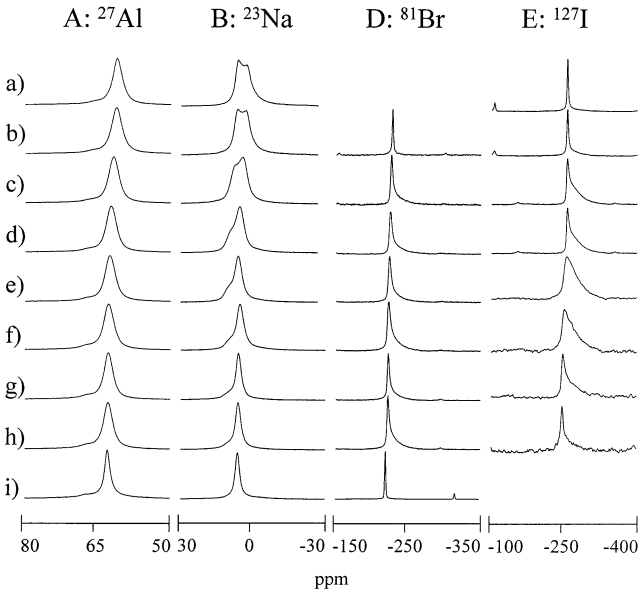

Figure 6. ^{23}Na, ^{27}Al, ^{81}Br, and ^{127}I MAS NMR spectra of mixed Br/I sodalites. The spectra were taken in a 11.7 T magnetic field at spinning speeds of 10 kHz. The sodalite cages are over 98% occupied by halide ions of which (a) 0%, (b) 6%, (c) 25%, (d) 46, (e) 65%, (f) 77%, (g) 86%, (h) 91%, and (i) 100% are Br^-.

Two sodium resonances are also observed in the Br/I series, albeit less well resolved. Again, the corresponding halide fractions can be extracted from simulated line shapes. The quadrupolar coupling parameter P_Q for sodium in bromo cages is 0.8 MHz, similar to that for the Cl/Br series. For sodium in iodo cages, P_Q is 1.75 MHz and increases to 2.1 MHz for sodalites containing little iodine. These quadrupolar parameters can be deduced from TQ MAS spectra, such as shown in Figure 8a, where the two spectral components are clearly separated.

As already mentioned, Cl/I sodalites do not form solid solutions over a wide compositional range. Nevertheless, the ^{23}Na MAS NMR spectra of the samples with very high and very low Cl contents show the same trends in intensities, chemical shifts, and P_Q values as do the ^{23}Na NMR spectra of

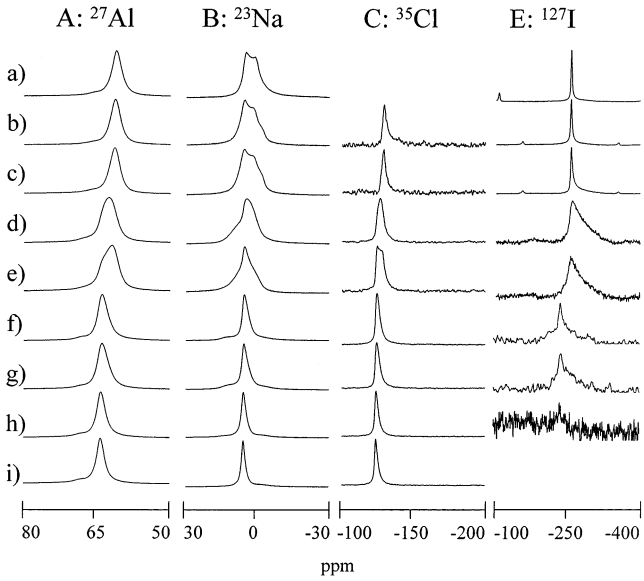

Figure 7. ^{23}Na, ^{27}Al, ^{35}Cl, and ^{127}I MAS NMR spectra of mixed Cl/I sodalites. The spectra were taken in a 11.7 T magnetic field at spinning speeds of 10 kHz. The sodalite cages are over 98% occupied by halide ions of which (a) 100%, (b) 95%, (c) 94%, (d) 89, (e) 78%, (f) 11%, (g) 10%, (h) 3%, and (i) 0% are I^-.

the other series. For the 25% Cl containing mixed Cl/I sodalite, the ^{23}Na TQ MAS NMR spectrum in Figure 8b clearly resolves the two distinct environments. The broad line shape of the sodium ions in the I-bearing cages cannot be fitted accurately in 1D spectra, thus all of the NMR parameters in this series had to be determined by TQ MAS.

^{23}Na NMR shieldings and electric field gradients were also calculated by GAUSSIAN98, as described in the Experimental Section. These calculations were applied to six-ring arrangements with chlorine, bromine, and iodine centers, as well as with empty cages. The shielding values are given in Table 2 and are easily converted to chemical shifts according to eq 5. For dry sodalite, our ^{23}Na shieldings are on the order of 10 ppm smaller than those previously calculated by Tossell for slightly different structural models[9,10]

$$\delta = (\sigma_{ref} - \sigma) \tag{5}$$

The NMR shielding of a sodium ion coordinated by six water molecules was chosen as the reference point in our calculations. The equilibrium Na−O distances calculated are 2.383 Å and result in an absolute shielding $\sigma_{ref} = 578$ ppm. This value differs significantly from Tossell's recent result of 588.9 ppm calculated with Gaussian-94. The absolute shielding of a free sodium ion amounts to 631 ppm. The calculations reveal that, at fixed Na−halogen distance, the ^{23}Na nucleus is increasingly deshielded with increasing mass of the halogen ion, in agreement with the experimental data. We also find that the ^{23}Na chemical shift shows a monotonic dependence on the lattice constant for each of the two sites observed in the three series.

The experimentally determined ^{23}Na quadrupolar coupling constant increases with the mass of the nearby halide anion from 0.4 MHz for the sodium in chloro sodalite cages to 1.75 MHz for sodium in iodo sodalite cages. This is in good agreement with values determined previously from SATRAS NMR spectroscopy.[16] This trend is not revealed by the ab initio calculations, however. Moreover, the computed C_Q-values are found to be highly sensitive to the Na−halogen distance at variance with the experimental findings. We ascribe these discrepancies to the intrinsic limitations of the theoretical model, which lacks

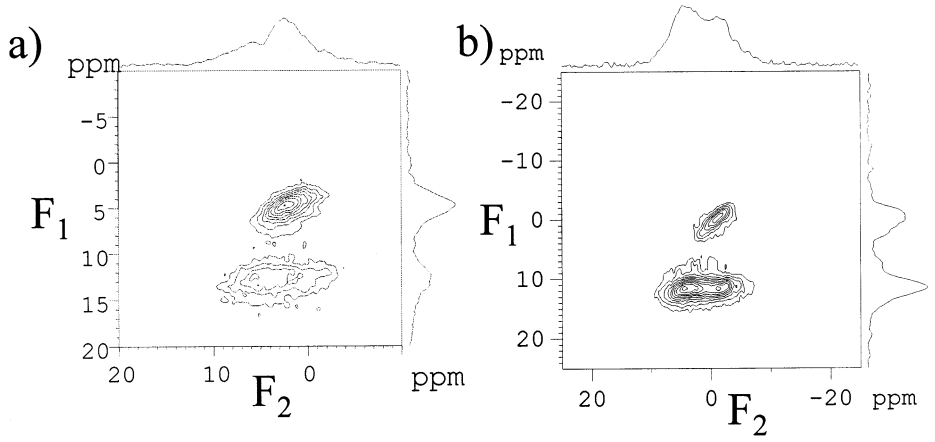

Figure 8. ^{23}Na TQ MAS NMR spectra of (a) Br/I−sodalite solid solution containing 65% Br^- (corresponding to Figure 6e) and (b) Cl/I−sodalite solid solution containing 94% I^- (corresponding to Figure 7c) at a MAS frequency of 15 kHz and magnetic field strength of 11.7 T

TABLE 2: ^{23}Na Shieldings Calculated as a Function of Na−Halogen Distances as Described in the Text[a]

	cell parameters		^{23}Na isotropic shieldings		
a_0, Å	r(Na−Hal), Å	Na−Cl, ppm	Na−Br, ppm	Na−I, ppm	Na dry, ppm
		r(Na−O) = 2.355 Å			
8.800	2.548	572.24	563.81	551.15	584.71
8.850	2.656	575.14	568.07	559.54	584.76
8.900	2.773	577.41	571.58	566.45	584.70
8.950	2.902	579.34	574.56	572.03	584.60
9.000	3.049	581.16	577.24	576.46	584.62
9.050	3.220	582.98	579.81	579.90	584.85
9.100	3.439	584.79	582.50	582.53	585.30
		r(Na−O) = 2.330 Å			
8.800	2.602	572.28	564.59	553.54	583.10
8.850	2.714	574.76	568.36	561.09	583.05
8.900	2.836	576.87	571.52	567.25	582.92
8.950	2.971	578.59	574.28	572.18	582.85
9.000	3.127	580.36	576.83	576.04	582.95
9.050	3.315	582.13	579.38	579.02	583.27
9.100	3.575	583.90	582.15	581.32	583.81

[a] All ionic positions were derived from the lattice constant a_0 and fixed Na−O distances of 2.355 and 2.330 Å (see text).

appropriate charge balance needed to produce more accurate results. A sufficiently charge balanced environment would require more than 100 atoms, which is beyond our computational limits.

Halogen MAS NMR. All the ^{35}Cl MAS NMR spectra of the chloride-containing mixed sodalite series show (with one exception) a single resonance (see Figures 5C−7C). The chemical shifts observed vary between −123.9 and −128.7 ppm for pure chloro sodalite and 5% chloride containing iodo sodalite, respectively. The line shapes are in all cases nearly symmetric, and the field-dependent measurements reveal that the quadrupolar couplings are rather weak ($C_Q = 0.4 \pm 0.3$ MHz). For pure chloro sodalite a P_Q value of 55 ± 5 kHz was estimated from the satellite transition spinning sideband manifold (SATRAS) as displayed in Figure 9a. In the case of 50% Cl containing mixed Cl/I sodalite, two main resonances with chemical shifts of 127.6 and 124.6 ppm were resolved by ^{35}Cl TQ MAS NMR, suggesting the existence of two separate regions or phases in agreement with the segregated character of this sample. A distribution of chemical shifts between these values can be noted as well, consistent with the occurrence of domains with intermediate compositions.

The ^{81}Br NMR spectra of all Br-containing sodalites in Figures 6D and 7D also show only one resonance. The chemical shifts of these resonances depend on the sodalite composition

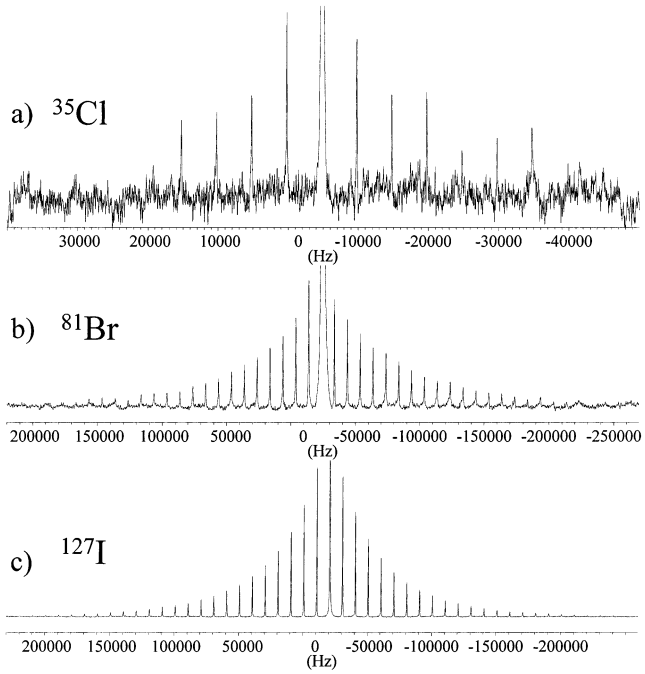

Figure 9. SATRAS NMR spectra of the pure halide sodalites: ^{35}Cl at 39.19 MHz, ^{81}Br at 108.03 MHz, and ^{127}I at 80.03 MHz. A probe with a low quality factor was used, to ensure signal acquisition at frequency offsets up to ±1 MHz from the resonance center. The central resonance amplitudes are off scale to reveal the weaker spinning sideband manifolds generated by the effect of MAS on the first-order quadrupolar satellite powder patterns.

and vary between −217.4 and −227.8 ppm for low Br-containing chloro and iodo sodalites, respectively. Except for pure bromo sodalite, all lines show a low-frequency asymmetry, which becomes more pronounced with decreasing bromine content. The P_Q values also increase with decreasing bromine content and vary between 0.5 and 0.9 MHz. These represent average values, since the line shape indicates a distribution of quadrupolar coupling constants. The values given here were deduced from the peak positions measured at 9.4 and 11.7 T, using eq 2. The SATRAS spectrum of pure bromo sodalite in Figure 9b indicates a distribution of P_Q values around a mean value of 0.4 MHz.

The ^{127}I spectra (Figures 6E and 7E) reveal the strongest dependence on composition. While the chemical shift varies between −236 and −256 ppm within the range of the samples studied, the ^{127}I line shape proves extremely sensitive to the composition of the sample. For pure iodo sodalite, the line width

is 270 Hz, but it increases to more than 4000 Hz for 50/50 mixed Cl/I and Br/I sodalites. For low iodine concentrations, the line widths decrease to about 1000 and 400 Hz in the case of Cl/I and Br/I sodalites, respectively. A similar trend is observed in the P_Q parameters, which vary between 0.4 ± 0.2 and 4 ± 2 MHz throughout these series. The ^{127}I SATRAS spectrum in Figure 9c indicates a distribution of P_Q values for the pure iodo sodalite around a mean value of 0.8 MHz.

IV. Discussion

Control of the Mixed Sodalite Stoichiometry. As can be seen from Figure 4, only in the case of mixed Cl/Br sodalites the halide fractions in the sodalite lattices are closely related to the corresponding fractions in the precursor solution. Larger deviations are found in mixed Cl/I and Br/I sodalites. While the sodalite lattice itself is capable of hosting anions of unlike sizes, the solid solution with different halogen anions creates a strain in the sodalite framework. The latter arises from the fact that sodalite cages are face-sharing. Thus the same set of T−O-T angles in a hexagonal ring is part of two cages with different central anions. The larger the difference in the sizes of the central anions, the more likely are the deviations from their random distribution in the sodalite lattice. Instead, the same species may be preferably incorporated during the lattice growth, eventually leading to domain formation or a total phase separation. In the case of Cl/I sodalites, we observe that the dominant halide in the precursor is overrepresented in the sodalite, while for a 1:1 ratio the outcome seems to be somewhat random. As in the case of mixed ClO_4/OH sodalite,[17] the entropy gain associated with anion mixing cannot compensate for the strain release of the sodalite lattice achieved by the phase separation. Br/I sodalites also show an overrepresentation of the iodine species for bromide fractions in the precursor solution that are smaller than 0.25. At higher Br^- content the bromine incorporation is preferred.

The selectivity constants extracted from Figure 4 are only valid for the particular set of synthesis parameters. For Cl/I sodalites the partial mutual solubility found at 180 °C within the present study changes to complete phase separation when the synthesis temperature is lowered to 120 °C, as indicated by split X-ray reflections as well as two aluminum resonances corresponding to the lattices of nearly pure I and Cl sodalites. This is not surprising considering the significantly smaller $T\Delta S$ term at this temperature. It is further interesting to note that the inclusion of smaller halogen anions is preferred for sodalites synthesized at 95 °C,[18] while no preferences are found for sodalites prepared from high-temperature solid-state reactions.[5] This clearly indicates that the synthesis at sufficiently high temperatures can overcome any enthalpic preferences for anions of certain sizes and will result in the entropy-favored, thermodynamically most stable solid solutions. From the present study we can conclude that at 180 °C the formation of mixed sodalites is still controlled by enthalpic effects due to the different sizes of the sodalite cages. The preferred cage size appears to be somewhere between the values of pure chloro and pure bromo sodalite. This would explain the symmetry of chlorine and bromine intake, while in the Br/I case bromine incorporation is preferred. The inability of forming Cl/I sodalite solid solutions over the whole concentration range is then due to the different size requirements of both halide ions, which cannot be overcome energetically below 180 °C.

Solid Solution Effects on the Framework and on the Extraframework Ions. As described previously,[11−13] the measured cubic lattice constants can be translated into corresponding changes in mean T−O−T angles and Na−halogen distances, respectively. The discussion to follow will focus on how the trends observed for these parameters in these solid solution series will affect the chemical shift and nuclear electric quadrupole coupling constant values. The fact that only single ^{27}Al resonances are observed for all the mixed sodalites in this study indicates that the central anions have a negligible effect on the electronic environment of the framework atoms. While the P_Q values for all aluminum resonances scatter around 0.8 MHz, the chemical shifts follow the established correlation with T−O−T bond angles[19] described by $\delta = 168 - 0.74$ ppm/Å (see Figure 10).

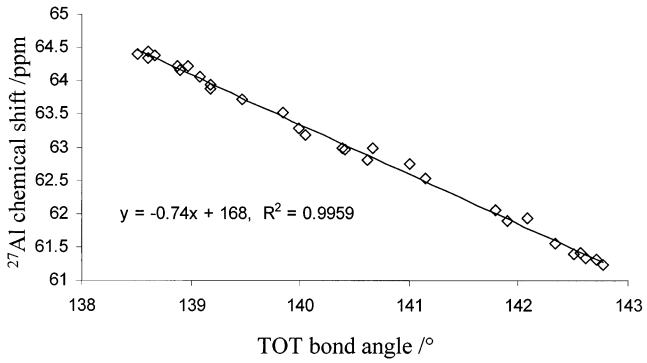

Figure 10. ^{27}Al NMR chemical shifts as a function of the TOT bond angle, derived from the lattice constant in all of the samples investigated. The solid line represents a linear least-squares fit through the data.

The most significant structural aspect contained in the chemical shift data of this study concerns the interactions among the sodium and the halogen ions. The sodium ions in halogen sodalites are coordinated by three framework oxygen atoms, which are all part of the same hexagonal window, and the halogen anion at the cage center. Since the Na−O distance for the pure halogen sodalites is always 2.355 ± 0.005 Å,[5] it is reasonable to assume that this holds for mixed halogen sodalites as well. In this case, the Na−halogen distances are exclusively controlled by the lattice constant a_o,[11] which for mixed halogen sodalites varies between 8.893 and 9.012 Å. This range of lattice constants translates into Na−halogen distance variations between 2.7 and 3.07 Å in these solid solutions, thereby providing a unique opportunity to explore the fundamental relationship between the chemical shifts of the ^{23}Na and the halide resonances and the Na−halogen interionic distances.

Interpretation of the ^{23}Na Chemical Shift Trends in Mixed Sodalites. It has been generally established that the magnitude of the (dominant) paramagnetic deshielding effect in ionic materials arises from the extent of anion−cation overlap.[20] For the pure alkali halide salts, Hafemeister and Flygare[21] have conducted Hartree−Fock calculations of the outer shell overlap integrals of the alkali and halide ions, yielding the following empirical relation

$$S_{ab} = Ce^{-r/\rho} \tag{6}$$

where S_{ab} is the overlap integral, r is the interatomic distance, and C and ρ are empirical constants. According to Hafemeister and Flygare the chemical shielding is then a function of the sum of squared overlap integrals involving all overlapping outer orbitals and can also be described by an exponential decay. An exponential dependence of δ_{iso} on bond distance was also found experimentally by Xue and Stebbins.[22] Recently Tossell[9,10] has shown that the ^{23}Na NMR shielding can be reliably computed by the Restricted-Hartree−Fock method applying rather simple

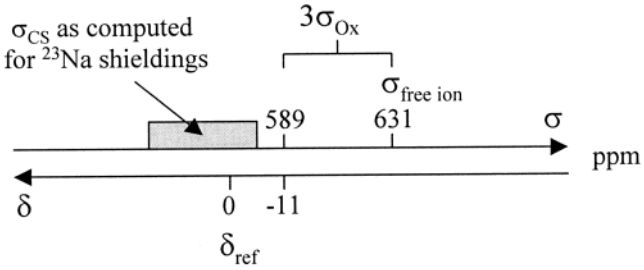

Figure 11. Relation between calculated shieldings (σ) and observed shifts for the ^{23}Na environments. $\sigma_{fi} + 3\sigma_{Ox} = 589$ ppm and $\delta_0 = +11$ ppm are the offsets of the exponential fits in the calculated shieldings and the experimental shifts, respectively, representing the values for the sodalite environment without the halide ion.

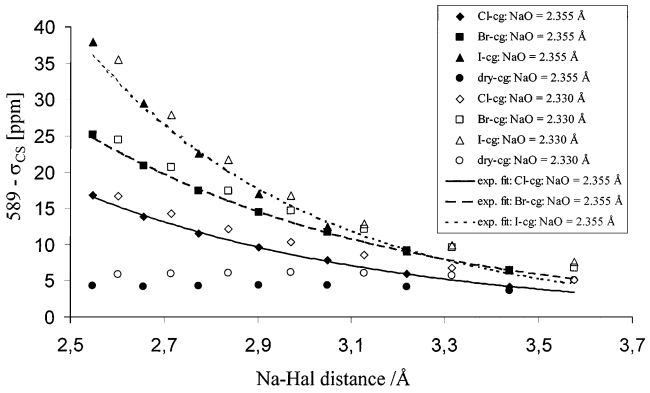

Figure 12. Computed ^{23}Na chemical shifts for sodium in (circles) empty, (diamonds) Cl-, (squares) Br-, and (triangles) I-occupied cages. Filled symbols show shieldings calculated on the basis of Na−O distances of 2.355 Å, whereas the open symbols display shieldings calculated on the basis of Na−O distances of 2.330 Å (see text). The curves show fits to eq 7.

basis sets. Also, the shielding of a ligand environment could be successfully computed by summation of the shielding contributions of every single ligand, while no significant angular dependence was observed. Based on these ideas and on the assumption that the sodium−oxygen distance remains at a constant value of 2.355 Å for all our samples, we can separate the different shielding contributions in order to identify the influence of the Na−halogen distance on the sodium shielding

$$\sigma_{cs} = \sigma_{fi} + 3\sigma_{Ox} + A_{NaHal}e^{-r/r_{0NaHal}} \quad (7)$$

Here σ_{fi} is the absolute shielding of the free sodium ion and $3\sigma_{Ox}$ is the shielding contribution due to the three oxygen ligands, A_{NaHal} and r_{0NaHal} are ligand dependent constants, and r is the distance between sodium and the halide ion. A_{NaHal} and $3\sigma_{Ox}$ represent paramagnetic deshielding contributions and are thus negative in sign. To compare experiment with theory we use eq 7, which separates the shielding contribution dependent on the Na−Hal distance from all other contributions.

According to our calculations, the shielding of the free sodium ion is 631 ppm and the contribution of the oxygen atoms was found to be −42 ppm, resulting in $\sigma_{fi} + 3\sigma_{Ox} = 589$ ppm (see Figure 11).

Figure 12 thus plots 589 ppm $-\sigma_{CS}$ versus the Na−halogen distance for the three series investigated, resulting in fitting parameters of A and r_0 listed in Table 2. Included in this figure are also shielding values calculated on the basis of the Na−O distance of 2.330 Å as found in dehydrated salt-free sodalite at room temperature.[11,23] Very similar results are obtained indicating that typical variations in the Na−O distances observed in different sodalite systems would only exert a minor influence on the ^{23}Na chemical shifts. Figure 12 further includes ^{23}Na shielding values calculated for dry salt-free sodalite cages (no halide ions present). As expected, the quantity (589 ppm $-\sigma_{CS}$) is found close to zero in this case (the slight deviation can be attributed to a minor influence of Na^+ neighbors within the cage, which now is not screened by the halide ion). We also calculated the sodium shielding for Na-halogen "molecules" disregarding the oxygen environments. Even in this simplified model the trends are followed and the corresponding fitting parameters are given in Table 3. In addition, Table 3 contains the exponential fitting parameters to eq 6 to the sums of squared overlap integrals calculated by Hafemeister and Flygare.

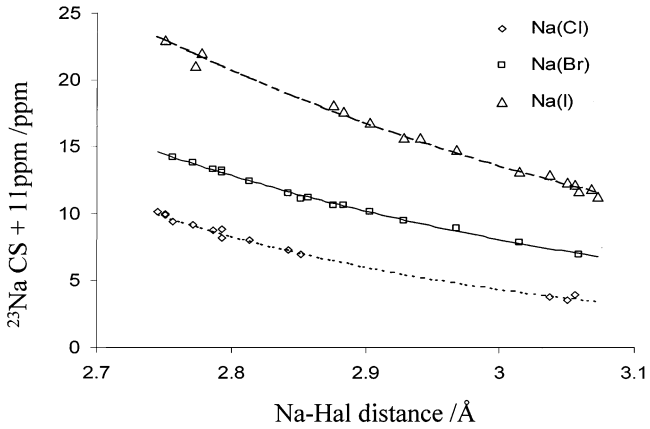

Figure 13. Experimental ^{23}Na chemical shifts as a function of Na−halogen distance for all of the single-phase samples under investigation. The shifts plotted include a 11 ppm correction for the oxygen ligands, as described in the text. The curves show fits to eq 8.

TABLE 3: Exponential Fitting Parameters for the Na−Halogen-Dependent Part of the Sodium Shieldings for the Three Types of Halide Cages in the Samples under Study. Literature Values for the Anion−Cation Overlap Integral in Alkali Halide Salts with Rock Salt Structure are also Included

	NaCl		NaBr		NaI	
distance dependence of	$-A$, ppm	r_0, Å	$-A$, ppm	r_0, Å	$-A$, ppm	r_0, Å
δ_{iso} (exp)	1260	0.63	1110	0.68	1930	0.65
δ_{iso} (GAUSS. 6-ring)	800	0.65	1120	0.67	5900	0.51
δ_{iso} (GAUSS. NaHal)	3100	0.57	3200	0.61	1300	0.78
ΣS^2 (ref 21)	51	0.35	32	0.36	31	0.38

Experimentally, chemical shifts rather than absolute shieldings are measured. Thus eq 7 turns into

$$-\delta_{CS} = \sigma_{cs} - \sigma_{ref} = [\sigma_{fi} + 3\sigma_{Ox} - \sigma_{ref}] + A_{NaHal}e^{-r/r_{0NaHal}} \quad (8)$$

The experimental δ_{CS} values measured for all three mixed halide sodalite series can be fitted to eq 8 by fixing the value in the brackets to 589−578 = 11 ppm, yielding $\delta_{CS} + 11$ ppm $= -A \exp -\{r/r_0\}$ (see Figure 13). Table 3 includes the corresponding fitting parameters for A and r_0 from the experimental data. For sodium in chloro and bromo cages the agreement with the computational data is quite good, especially in view of the fact that the fitting results are very sensitive to the chosen offset values.

Both the experimental and the calculated data reveal that the deshielding caused by the halide at a fixed distance increases with atomic number and decreases with increasing Na−halogen distance. This effect becomes more pronounced with increasing atomic number of the halide ion. Overall the trends in the

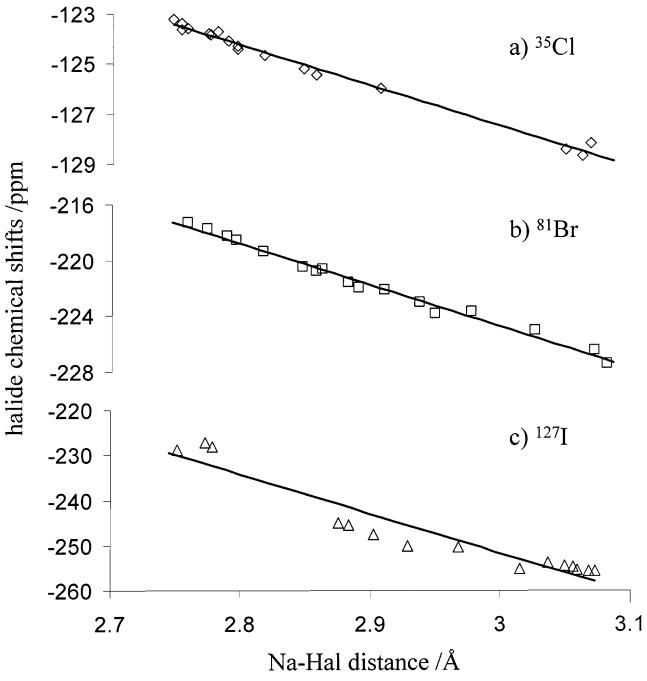

Figure 14. Experimental NMR chemical shifts of ^{35}Cl, ^{81}Br, and ^{127}I as a function of Na−halogen distance for all of the single-phase samples under investigation. The lines represent linear least-squares fits to the data.

magnitude of the computed deshielding contributions are in good agreement with the experimental results. The computed ^{23}Na shieldings for iodo sodalites, however, deviate from the experimental data. We attribute this to the limitations of the non relativistic basis set SDD used in these calculations.

The summed squared overlap integrals, which should be proportional to the shielding, generally show much smaller characteristic lengths r_0. However, they have been tested only for the equilibrium interatomic distances in the halide salts, where they lead to qualitative agreement with the absolute shielding values found experimentally.[21] To date, the only distance-dependent data interpreted in this vein have been pressure-dependent resonance shifts of Rb and Cs halide salts.[24]

Halide Chemical Shift Trends in the Mixed Sodalites. Concerning the halide resonances, the chemical shifts compared to the 1 M aqueous solutions decrease from −123.5 ppm for ^{35}Cl to −220.6 ppm for ^{81}Br, to −256 ppm for ^{127}I. Since we do not have experimental estimates for the chemical shifts of all the free halide ions, exponential fits of δ vs Na−halogen distance curves would lead to arbitrary values for A_i, r_{0i}, and δ_0. Therefore we have simply fitted the halide chemical shifts plotted in Figure 14 with linear expressions, the slopes of which increase from ^{35}Cl to ^{81}Br and further to ^{127}I, roughly by factors of 2 (from 17 to 35 to 75 ppm/Å, respectively). The increase of chemical shift sensitivity with increasing atomic number is in good accord with known experimental trends in the Periodic Table.

The halogen anions in the centers of the sodalite cages might also be viewed as molecular fragments present in hypothetical halide salt polymorphs with tetrahedral (instead of octahedral) coordination geometry. Thus we may compare the chemical shifts of the sodalite halides, corrected for their different Na−halogen distances by the linear fits from Figure 14, to the chemical shifts of the rock-salt like halide salts. The differences ($\delta_{salt} - \delta_{SOD}$) of 77.8, 210.5, and 456.6 ppm for ^{35}Cl, ^{81}Br, and ^{127}I, respectively, indicate that the shielding in the rock salt structures is much more paramagnetic than in the isolated tetrahedral fragments. The origin of this large effect can be identified with the strong anion−anion overlap (which is absent in the sodalites) but produces a strong deshielding contribution in the binary salt compounds.[20,25,26] An analogous conclusion was drawn from a comparison of ^{129}I Mössbauer data obtained on alkali iodide salts and those of the corresponding matrix-isolated molecules.[27] The large increase of ($\delta_{salt} - \delta_{SOD}$) within the series Cl → Br → I can be attributed to a dramatic increase of the anion−anion overlap effect with increasing atomic number of the halide.

V. Conclusions

We have investigated the formation of the mixed halogen sodalites synthesized under hydrothermal conditions, which allows the controlled preparation of the sodalites with desired stoichiometry. For the Cl/I system a "solubility" gap was found between 15% and 85% of either species at synthesis temperatures of 180 °C, while Cl/Br and Br/I mixed halide sodalites form solid solutions over the whole concentration range at this temperature.

We have further characterized these sodalites structurally by multinuclear NMR spectroscopy. The ^{27}Al NMR data confirm the previously established relation between the ^{27}Al chemical shift and the T−O−T bond angle. The ^{23}Na and halide NMR data represent the first systematic study of chemical shift as a function of Na−halogen distance without the application of elevated pressures or temperatures. For sodium we find an exponential relation in accordance with theoretical predictions based on the extent of anion−cation wave function overlap. The chemical shifts of ^{35}Cl, ^{81}Br, and ^{127}I are also sensitive to anion−cation overlap and their sensitivity to distance increases with increasing atomic number of the halogen. These results offer new insights into the nature of the nuclear magnetic shielding in compounds with predominantly ionic bonding.

Acknowledgment. We thank Galen D. Stucky for the use of X-ray facilities and the Deutsche Forschungsgemeinschaft as well as the USA National Science Foundation (NSF) for their financial support. Partial funding by SFB 458 and the Wissenschaftsministerium Northrhine Westphalia is most gratefully appreciated.

References and Notes

(1) Bibby, D.; Dale, P. *Nature* **1985**, *317*, 157−158.
(2) Depmeier, W. *Acta Crystallogr.* **1984**, *B40*, 185−191.
(3) Pauling, L. *Z. Kristallogr.* **1930**, *74*, 213.
(4) Barrer, R. M.; Cole, J. F. *J. Chem. Soc. A* **1970**, 1516−1523.
(5) Weller, M. T.; Wong, G. *Eur. J. Solid State Inorg. Chem.* **1989**, *26*, 619−633.
(6) Frydman, L.; Harwood, J. S. *J. Am. Chem. Soc.* **1995**, *117*, 5367.
(7) Amoureux, J. P.; Fernandez, C.; Steuernagel, S. *J. Magn. Reson.* **1996**, *A 123*, 116.
(8) Frisch, M. J.; Trucks, G. W.; Schlegel, H. B.; Scuseria, G. E.; Robb, M. A.; Cheeseman, J. R.; Zakrzewski, V. G.; Montgomery, J. A.; Stratmann, R. E.; Burant, J. C.; Dapprich, S.; Millam, J. M.; Daniels, A. D.; Kudin, K. N.; Strain, M. C.; Farkas, O.; Tomasi, J.; Barone, V.; Cossi, M.; Cammi, R.; Mennucci, B.; Pomelli, C.; Adamo, C.; Clifford, S.; Ochterski, J.; Petersson, G. A.; Ayala, P. Y.; Cui, Q.; Morokuma, K.; Malick, D. K.; Rabuck, A. D.; Raghavachari, K.; Foresman, J. B.; Cioslowski, J.; Ortiz, J. V.; Baboul, A. G.; Stefanov, B. B.; Liu, G.; Liashenko, A.; Piskorz, P.; Komaromi, I.; Gomperts, R.; Martin, R. L.; Fox, D. J.; Keith, T.; Al-Laham, M. A.; Peng, C. Y.; Nanayakkara, A.; Challacombe, M.; Gill, P. M. W.; Johnson, B.; Chen, W.; Wong, M. W.; Andres, J. L.; Gonzalez, C.; Head-Gordon, M.; Replogle, E. S.; Pople, J. A. *Gaussian98*; A.9 ed.; Gaussian Inc.: Pittsburgh, PA; 2000.
(9) Tossell, J. A. *Phys. Chem. Miner.* **1999**, *27*, 70−80.
(10) Tossell, J. A. *J. Phys. Chem. B* **2001**, *105*, 11060.
(11) Hassan, I.; Grundy, H. D. *Acta Crystallogr.* **1984**, *B40*, 6−13.
(12) Shannon, S. R.; Campbell, B. J.; Metiu, H.; Blake, N. P. *J. Chem. Phys.* **2000**, *113*, 10 215−10 225.

(13) Trill, H.; Eckert, H.; Srdanov, V. I. *J. Am. Chem. Soc*. **2002**, *124*, 8361−8370, Trill, H. Sodalite Solid Solution System. Synthesis, Topotactic Transformations, and Investigation of Framework-Guest and Guest−Guest Interactions. Ph.D. Thesis, Westfälische Wilhelms Universität: Münster, 2002.

(14) Samoson, A. *Chem. Phys. Lett.* **1985**, *119*, 29.

(15) Engelhardt, G.; Kentgens, A. P. M.; Koller, H.; Samoson, A. *Solid State Nucl. Magn. Reson.* **1999**, *15*, 171−180.

(16) Nielsen, N. C.; Bildsoe, H.; Jakobsen, H. J.; Norby, P. *Zeolites* **1991**, *11*, 622−632.

(17) Engelhardt, G.; Sieger, P.; Felsche, J. *Anal. Chim. Acta* **1993**, *283*, 967−985.

(18) Cocks, P.; Pope, C. *Zeolites* **1995**, *15*, 701−707.

(19) Jacobsen, H. S.; Norby, P.; Bildsoe, H.; Jakobsen, H. J. *Zeolites* **1989**, *9*, 491−495.

(20) Kondo, J.; Yamashita, J. *J. Phys. Chem. Solids* **1959**, *10*, 245.

(21) Hafemeister, D.; Flygare, W. *J. Chem. Phys.* **1965**, *43*, 795−800.

(22) Xue, X.; Stebbins, J. F. *Phys. Chem. Miner*, **1993**, *20*, 297.

(23) Campbell, B. J.; Delgado, J. M.; Cheetham, A. K.; Iversen, B. B.; Blake, N. P.; Shannon, S. R.; Latturner, S.; Stucky, G. D. *J. Chem. Phys.* **2000**, *113*, 10226−10239.

(24) Baron, R. *J. Phys. Chem.* **1963**, *38*, 173−187.

(25) Yamagata, Y. *J. Phys. Soc. Jpn*. **1964**, *19*, 10.

(26) Sears, R. E. J. *J. Chem. Phys*. **1977**, *66*, 5250.

(27) Pasternak, M.; Shamai, S. *J. Chem. Phys*. **1977**, *66*, 3924